PAPER

Check for updates

Surface modification of magnetic nanoparticles by bacteriophages and ionic liquids precursors†

Paweł Działak, [ID] *[a] Marcin Daniel Syczewski,[bc] Artur Błachowski, [ID] [a] Kamil Kornaus,[d] Tomasz Bajda, [ID] [a] Łukasz Zych,[d] Magdalena Osial[e] and Andrzej Borkowski [ID] [a]

Magnetic nanoparticles (MNPs) have recently been a point of interest for many researchers due to their properties. However, the studies on the influence of bacteriophages on the synthesis of MNPs seem to be lacking. Furthermore, bacteriophage-modified MNPs have not been combined with *n*-alkyl quaternary ammonium ionic liquid precursors (QAS). In this study, the aim was to assess the influence of two distinctly different bacteriophages (*Escherichia* phage P1 and *Pseudomonas* phage Φ6) on MNPs synthesis in the presence or absence of QAS. Synthesized MNPs have been characterized with X-ray diffraction (XRD) and Mössbauer spectroscopy in terms of changes in the crystallographic structure; scanning electron microscopy (SEM) for changes in the morphology; and ζ-potential. Moreover, the sorption parameters and the loss of viability of bacteria that interacted with MNPs have been determined. The sorption of bacteria differs significantly among the tested samples. Furthermore, the viability of the bacteria adsorbed on MNPs varies in the presence of QAS, depending on the length of the *n*-alkyl chain. The study has revealed that MNPs can be bound with bacteriophages. Mössbauer spectroscopy has also revealed the probable influence of bacteriophages on the formation of crystals. However, these phenomena require further studies.

1.   Introduction

Magnetite and maghemite are ferrimagnetic iron oxide nanoparticles (MNPs).[1] MNPs have been widely used in the medical field due to their biocompatibility, biodegradability, and perfect superparamagnetic properties.[2] The magnetic or electrochemical properties of magnetic nanoparticles differ significantly from bulk precipitates.[3] MNPs have been used mainly as contrast agents for MRI diagnostics[4,5] and targeted drug delivery in cancer treatments.[6,7] Green synthesized magnetite nanoparticles have been proposed as adsorbents for the efficient removal of Cr(VI).[8] Furthermore, there are reports on the synthesis of biogenic magnetite nanoparticles and their ability to remove azo dyes and phenolic contaminants from water.[9] Maghemite nanoparticles have also been used in similar ways.

[a]Faculty of Geology, Geophysics and Environmental Protection, AGH University of Science and Technology, Al. Mickiewicza 30, 30-059 Krakow, Poland. E-mail: dzialak@agh.edu.pl

[b]Helmholtz Centre Potsdam, GFZ German Research Centre for Geosciences, D-14473 Potsdam, Germany

[c]Faculty of Geology, University of Warsaw, ul. Żwirki i Wigury 93, 02-089 Warsaw, Poland

[d]Faculty of Materials Science and Ceramics, AGH University of Science and Technology, Al. Mickiewicza 30, 30-059 Krakow, Poland

[e]Institute of Fundamental Technological Research, Polish Academy of Sciences, Pawińskiego 5B, 02-106 Warsaw, Poland

† Electronic supplementary information (ESI) available. See DOI: https://doi.org/10.1039/d2ra06661k

They have been applied to remove Cr(VI)[10] and Pb(II).[11] Interestingly, MNPs have also been used for magnetic hyperthermia in cancer treatments.[12] MNPs can be synthesized using many different methods, including mineral waste from the iron ore processing plant;[13] electrochemical techniques;[14] thermal decomposition in the presence of surfactants;[15] hydrothermally from iron(III) acetylacetonate;[16] from acid mine drainage sludge using sodium carbonate.[17] However, the most common is the co-precipitation of Fe^{2+} and Fe^{3+} by $NH_{3(aq)}$ or NaOH due to simplicity and cost effectiveness.[18–20] Magnetite nanoparticles can be oxidized to maghemite with ferric nitrate at elevated temperatures.[21] However, the magnetite–maghemite transformation can also occur at room temperature with exposure to air.[22] Moreover, MNPs can be coated with various chemical compounds. The coating can change the physicochemical properties of the surface.[23] There are reports on magnetite coatings with: chitosan and curcumin;[24] polyethylene glycol and sorafenib;[25] aminofunctional alkoxysilanes;[26] polyethylene glycol and polyols;[27] poly(acrylic acid);[28] cinnamaldehyde.[29] Furthermore, MNPs can also be attached to albumin.[30,31] Maghemite can also be coated with various compounds, among others: poly(*N*,*N*-dimethylacrylamide),[32] polyaniline,[33] methotrexate.[34] Maghemite nanoparticles can even be coated with bacteria.[35] Bacteriophages have not been used often as MNPs modifiers. Most importantly, bacteriophages have sizes similar to nanoparticles (50–100 nm), have the ability to form agglomerates, and can also differ in the structure of the capsid. Some

bacteriophages consist of a lipid membrane surrounding the capsids. It is postulated that bacteriophages may influence the formation of various minerals. Bacteriophages may induce vaterite formation,[36] and are also supposed to influence the size of crystallites.[36,37] With the above-mentioned properties, bacteriophages are potentially useful as modifiers of nanoparticles.

The properties mentioned above significantly facilitate the interactions with amphiphilic compounds, such as ionic liquids and their precursors. These compounds, often known as surfactants, can interact with a variety of surfaces depending on their structure. Ionic liquids (ILs) are considered green solvents and can be synthesized sustainably.[38] ILs are melted salts composed of cations and anions.[39] They are non-flammable, non-volatile, and recyclable.[40] Furthermore, ILs have a broad spectrum of applications.[41] They have been found to be useful as solvents for electrocatalysis;[42] dopants of polymers;[43] in biotechnology.[44] ILs can also change the biochemical and morphological properties of microorganisms.[45] Quaternary ammonium salts (QAS) are among the most widely used cations.[46] Ionic liquids derived from QAS reveal different antibacterial properties.[47] It was also shown that the quaternary ammonium-based ionic liquids can interfere with bacterial membrane depending on the cell wall structure and properties of lipopolysaccharide.[48,49]

In this study, *Escherichia* phage P1 and *Pseudomonas* phage Φ6 have been used as modifying agents during the synthesis of MNPs. Additionally, precursors of quaternary ammonium ionic liquids have been applied to modify the surface properties of bacteriophage-MNPs complexes. The characteristics of the obtained nanostructures were examined with ζ-potential measurements, X-ray diffraction (XRD), scanning electron microscopy (SEM), Mössbauer spectroscopy, and epifluorescence microscopy. In addition, bacteria sorption on MNPs and viability tests have been conducted (Fig. 1).

2. Materials and methods

2.1. Microorganisms and media

Escherichia coli (DSM-5698); *Pseudomonas syringae* van Hall (DSM-21482) and *Bacillus cereus* (ATCC 11778) were used as the viral hosts. *Escherichia coli* and *Pseudomonas syringae* are hosts for bacteriophages: *Escherichia* phage P1 (DSM-5757) and *Pseudomonas* phage Φ6 (DSM 21518), respectively, while *Bacillus cereus* is an example of a Gram-positive bacteria. TSB medium (Biomaxima) and bacteriological LAB-AGAR (Biomaxima) were used to prepare media. *Escherichia coli* and *Bacillus cereus* were cultured at 37 °C, while *Pseudomonas syringae* at 25 °C.

2.2. Preparation of bacteriophage cultures

Escherichia phage P1 and *Pseudomonas* phage Φ6 were cultured using the double-layer agar method[48] with our modifications.[37] The soft agar layer was scraped using a glass spreader and placed in a 50 mL polypropylene tube. To the collected soft agar layer, Tris–MgCl₂ buffer (20 mM Tris–HCl, 20 mM MgCl₂ × 6H₂O, pH 7.5) buffer was added (15 mL), and the tube was vigorously shaken using a vortex. The tube was centrifuged (4400×g) for 5 min at 4 °C to remove the agar. The supernatant was transferred to 2 mL polypropylene tubes and centrifuged (24 250×g) for 45 min at 4 °C. The supernatant was discarded, and each viral pellet was resuspended in 0.5 mL of 0.9% NaCl solution. The viral suspension was then filtered through a 0.22 μm syringe filter (regenerated cellulose) to remove possible bacterial debris. The quantification of the bacteriophage yield was performed using a multiplate reader (Varioskan LUX, Thermofisher) on 96-well UV plates. For the quantification of bacteriophages, the following formula was used:[50]

$$\text{virions per mL} = \frac{(A_{269} - A_{320}) \times 6 \times 10^{16}}{\text{number of bases/virion}}.$$

The number of bases: 93 601 (ref. 51) and 13 300 (ref. 52) for *Escherichia* phage P1 and *Pseudomonas* phage Φ6, respectively.

The concentration of both bacteriophages was standardized at 1×10^{10} virions per mL.

2.3. Synthesis of magnetic nanoparticles

2.3.1. Synthesis for physicochemical investigations. Synthesis was carried out using the modified protocol of Thanh *et al.*[55] The following solutions were prepared: 2130 mg (13.1 mmol) of anhydrous iron(III) chloride (FeCl₃, Sigma-Aldrich) dissolved in 200 mL of deionized water (ddH₂O); 800 mg (4
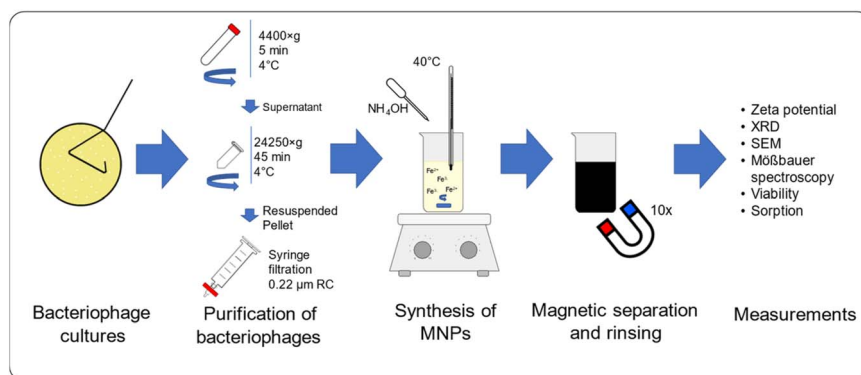

Fig. 1 Scheme of conducted experiments.

mmol) of tetrahydrate iron(II) chloride (FeCl$_2$·4H$_2$O, Sigma-Aldrich) dissolved in 100 mL of ddH$_2$O. For synthesis, the following solutions were used: 8 mL of FeCl$_3$, 4 mL of FeCl$_2$ and 1 mL of bacteriophage suspension (1×10^{10} virions per mL). For the control sample, instead of the bacteriophage solution, 1 mL of 0.9% NaCl solution was added. The solutions were placed in a beaker, stirred mechanically (600 rpm), heated up, and after reaching 40 °C, 1 mL of 25% NH$_3$(aq) was added dropwise until pH 11. The solution turned dark brown and was continuously stirred for 5 min. Subsequently, the nanoparticles were separated using a magnet (0.25 T), and the separated nanoparticles were rinsed 10 times with ddH$_2$O to remove the non-magnetic part, reagent residues and reach neutral pH. The following sample identification was used: (i) NP – magnetic nanoparticles, (ii) NP/P1 – magnetic nanoparticles with P1 bacteriophages, (iii) NP/Φ6 – magnetic nanoparticles with Φ6 bacteriophages. The nanoparticles obtained were stained with SybrGold® and observed under fluorescence microscopy (DM500 filter with a bandpass 460–490 nm excitation filter). Scanning Electron Microscopy (SEM) was conducted using a Carl Zeiss AURIGA (Carl Zeiss Microscopy GmbH). The samples were placed on a glass slide and coated with 20 nm layer of gold by a vacuum coater (Quorum 150T ES). Analysis was done with a 20 kV acceleration voltage.

2.3.2. Synthesis with ionic liquids precursors for viability tests.

Synthesis with *n*-alkyl quaternary ammonium ionic liquid precursors (QAS) (Table 1) was performed using the methodology described in Section 2.3.1 with modifications. A 6 mL portion of ferrous and ferric ions solution (4 mL FeCl$_3$ (426 mg 40 mL^{-1}) and 2 mL FeCl$_2$ (160 mg 20 mL^{-1})) was mixed with 5 mg of QAS (Table 1) and 0.5 mL of the bacteriophage suspension, or 0.9% NaCl solution (for nanoparticles without bacteriophages). Then, the mixed solution was heated to 40 °C, and 0.5 mL of 25%

NH$_3$(aq) was added. The QAS-modified nanostructures (NP/QAS) were rinsed 15 times to remove residues of ionic liquid precursors. The yield of the synthesis was max. 66 mg of MNPs. Before subsequent experiments, the suspensions of nanoparticles were air-dried. Subsequently, nanoparticle suspensions (20 mg mL^{-1}) in ddH$_2$O were prepared.

2.4. Loss of viability

A 20 µL aliquot of NP/QAS suspension (20 mg mL^{-1}) was mixed with 200 µL of bacteria (McFarland 5) in a 12-well microplate. Then, the incubation was carried out at 25 °C for 1 h. After incubation, 20 µL of the propidium iodide solution (2 mg 0.1 L^{-1}, pH 7.4) was added. After 5 min, 10 µL of the acridine orange solution (2 mg 0.1 L^{-1}, pH 7.4) was added. The stained suspension (20 µL) was placed on a microscopic slide with a cover slip, and analysed using the blue filter epifluorescence microscope (DM500 filter with a bandpass 460–490 nm excitation filter). Living bacteria are visualized in green, whereas dead or damaged microorganisms are in red. The 'loss of viability' of free-living bacteria and bacterial cells adsorbed on the surface of the nanoparticles was calculated using data collected from images with the following formula:

$$\text{Loss of viability} = \frac{\text{red stained cells}}{\text{green stained cells}} \times 100\%$$

The control viability was measured using the bacteria incubated without nanoparticles.

2.5. Viability of viruses attached to the nanoparticles

The viability test of viruses attached to the nanoparticles was carried out using the double-layer agar method described in

Table 1 The list of quaternary ammonium salts used in the synthesis of NP/QAS and applied nomenclature of the samples

Code of ionic liquid precursor	Ionic liquid precursor	Name of the sample
OH	Tetramethylammonium hydroxide pentahydrate (Sigma-Aldrich)	NP/OH NP/P1/OH NP/Φ6/OH
C8	Octyltrimethylammonium bromide (Fluka)	NP/C8 NP/P1/C8 C8/NP/Φ6
C10	Decyltrimethylammonium bromide (Fluka)	NP/C10 NP/P1/C10 NP/Φ6/C10
C12	Dodecyltrimethylammonium bromide (Acros-Organics)	NP/C12 NP/P1/C12 NP/Φ6/C12
C14	Tetradecyltrimethylammonium bromide (Acros-Organics)	NP/C14 NP/P1/C14 NP/Φ6/C14
C16	Hexadecyltrimethylammonium bromide (Acros-Organics)	NP/C16 NP/P1/C16 NP/Φ6/C16
C18	Trimethyloctadecylammonium bromide (Sigma-Aldrich)	NP/C18 NP/P1/C18 NP/Φ6/C18

Section 2.2. NP, NP/P1, and NP/Φ6 suspensions (20 mg mL^{-1}) were diluted serially (up to 10^{-9}). Then 100 µL of the diluted suspension was mixed with overnight *Escherichia coli* or *Pseudomonas syringae* cultures. Subsequently, the solution was mixed with the top agar and poured on the top of the solidified bottom agar.

2.6. ζ-Potential measurements

A 50 µL aliquot of the MNPs suspension (20 mg mL^{-1}) was diluted with 950 µL of ddH$_2$O and the suspension was placed in the measurement cell. The measurements were conducted with Zetasizer Nano-ZS (Malvern).

2.7. XRD

X-ray diffraction (XRD) data were determined using a Rigaku SmartLab diffractometer, with a graphite monochromator and rotating on a copper (Cu) anode. The data acquisition was in the range of 5–75° 2θ with a 0.05° gradation and a counting time of 1 s per grade.

2.8. Mössbauer spectroscopy

^{57}Fe Mössbauer spectroscopy measurements were performed in transmission geometry applying the RENON MsAa-4 spectrometer[56] equipped with the LND Kr-filled proportional detector. The He–Ne laser-based interferometer was used to calibrate a velocity scale. A commercial ^{57}Co(Rh) source made by RITVERC GmbH was used. The absorbers for the Mössbauer measurements were prepared using 15 mg cm^{-2} of investigated materials. The SVT-400 cryostat by Janis Research Inc. was used to maintain the absorber temperature. The Lorentzian approximation and the modified Hesse-Rübartsch method designed to extract hyperfine magnetic field distributions have been applied to fit Mössbauer spectra. The spectral isomer (center) shifts δ are reported concerning the isomer (center) shift of room temperature α-Fe.

2.9. Sorption

Langmuir isotherms were plotted to measure the sorption and affinity of bacteria to the modified MNPs. Bacterial suspensions (McFarland 6) were prepared and diluted 2×, 8×, 32×, and 128×. A 2 mL of the desired concentration of bacteria was placed in a 12-well microplate (in triplicate), and suspension of MNPs (containing 1 mg of MNPs) was added. The microplate was shaken horizontally (100 rpm) for 3 h at ambient temperature. Then, a 50 µL of 100× diluted SybrGold® dye and 50 µL of acridine orange (2 mg 100 mL^{-1}) were added. The nanoparticles were removed using a magnet, and 5 µL of the solution was placed in a Bürker chamber. All experiments were carried out in triplicate. The remaining cells were observed using an epifluorescence microscope fitted with a blue filter (DM500 filter with a bandpass 460–490 nm excitation filter). The remaining cells were automatically calculated with the Delta Optical DLT-CamViewer software. The average number of bacteria was obtained from 10 pictures for each sample. The Langmuir isotherms were fitted with non-linear least squares method (Statistica™, StatSoft).

The number of adsorbed bacteria (adsorbed cells per g) was calculated as follows:

$$n = \frac{(C_0 - C_{eq}) \times V}{m}$$

V – volume (5 mL), m – mass of the sorbent (0.001 g), C_0 – number of cells in the initial suspension (mL^{-1}), C_{eq} – number of bacteria remaining in the liquid phase after sorption (mL^{-1}).

The Langmuir equation is as follows:

$$n = \frac{(A_m \times K \times C_{eq})}{(1 + K \times C_{eq})}$$

where: A_m – maximum of adsorbed cells, K – Langmuir constant.

2.10. Statistical analysis

The Statistica 13 software (StatSoft Inc., Tulsa, OK, USA) was used for the statistical analysis. The following methods were used: one-way analysis of variance (ANOVA) at $p < 0.05$ with *post hoc* Scheffe and Dunnet tests for intergroup comparison; least number of squares for the nonlinear model for the Langmuir isotherms fitting.

3. Results

3.1. Magnetic nanoparticles and their characterization

The protocol for bacteriophage preparation allowed a very pure and dense suspension without bacterial debris to be obtained. The UV spectrum (Fig. S1†) showed a characteristic pattern with a maximum at 260 nm. The epifluorescence microscope after staining with SybrGold® showed that the bacteriophage suspension was free from bacterial cells (Fig. S2†). The behaviour (occurrence of agglomeration) of MNPs with and without bacteriophages was investigated using an optical microscope. Moreover, an epifluorescence microscope was used in order to highlight the presence of bacteriophages after SybrGold® staining.

Fig. 2 shows pairs of images (NP – 2a, b; NP/P1 – 2c, d; and NP/Φ6 – 2e, f) taken in bright field microscopy (left column) and epifluorescence microscopy (right column) for three samples. For the NP/P1 and NP/Φ6 samples, the capsids of bacteriophages were covered with MNPs, and were clearly visible after staining with SybrGold® (Fig. 2d and f). Bacteriophages were not visible in the optical microscopy images (Fig. 2c and e). The MNPs without bacteriophages were not visible under the epifluorescence (Fig. 2b), but the structure was visible in optical microscopy images (Fig. 2a).

The morphology of MNPs was investigated with SEM. However, the SEM images did not reveal any visible differences between the nanoparticles with and without bacteriophages (Fig. 3). Moreover, the single capsids of bacteriophages were not visible.

The crystallinity determination was performed using X-ray diffraction (XRD) analysis. Recorded X-ray diffraction patterns
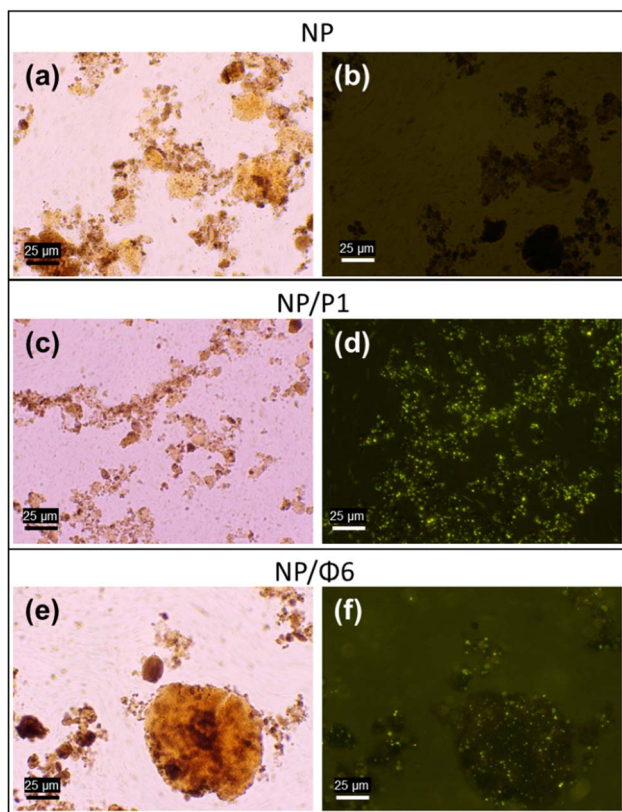
Fig. 2 Microscopic images of the magnetic nanoparticles after precipitation and purification (NP – a, b; NP/P1 – c, d; NP/Φ6 – e, f). Left column – light optical microscopy, right column – epifluorescence microscopy after SybrGold® staining.
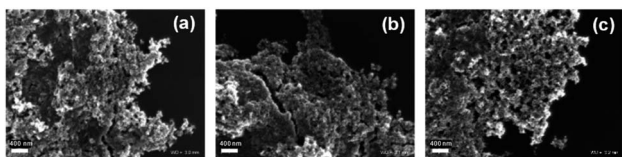

Fig. 3 SEM images of (a) – NP, (b) – NP/P1, and (c) – NP/Φ6.

revealed strong signals that can be attributed to maghemite and/or magnetite. This can be indicated by a slight shift of the peaks in relation to the reference peaks. It should be assumed that maghemite was present as the main phase in the sample, identified in the X-ray patterns from the presence of the 2.52, 1.47, 1.61, 2.95, 2.09, 1.70, and 4.82 Å reflections (Fig. 4). The other minerals were absent, or their content was below the sensitivity of the XRD analysis. The unit cell parameters (Table S1†) computed to compare the crystallite size did not reveal any significant differences. The parameters crystallite size only (Å or nm) can be considered the passage length of the diffraction radiation beam in a given lattice plane. These values are related to the size of the unit cell and show that there are essentially no differences between the examined minerals. For instance, at the first position (registered at 18.27, 18.297 and 18.299° 2θ for NP, NP/P1, and NP/Φ6, respectively) corresponding to the lattice
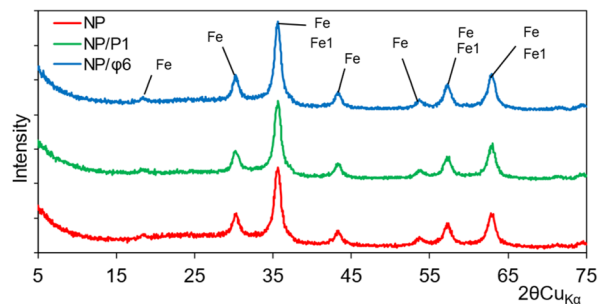

Fig. 4 XRD analysis of magnetic nanoparticles (NP), magnetic nanoparticles precipitated with P1 bacteriophages (NP/P1) and with Φ6 bacteriophages (NP/Φ6), where Fe – maghemite and Fe1 – magnetite.

plane (*hkl*) 1,1,1, crystallite size only was 4.81, 4.73 and 5.08 Å for the NP, NP/P1, and NP/Φ6, respectively. Similarly, it is possible to compare the microstrain only (%), which can be attributed to the degree of deformation of the crystal lattice. The values obtained did not differ substantially. However, it should be noted that the powder XRD allows only for approximate parameters of the unit cell.

^{57}Fe Mössbauer spectra of NP, NP/P1 and NP/Φ6 were recorded at room temperature (RT) and at 80 K. As shown in Fig. 5 and Table 2, the spectra contain two components at RT, and four at 80 K. The contributions of the respective spectral components are comparable between samples at a given temperature. At RT, about a quarter of the spectral area is a quadrupole doublet with the quadruple splitting $\Delta \approx 0.65$ mm s^{-1} and the isomer shift $\delta \approx 0.33$ mm s^{-1}, typical for maghemite nanoparticles.[57] It means that about a quarter of the Fe atoms are in the tiny nanoparticles, estimated to be well below 5 nm and exhibiting

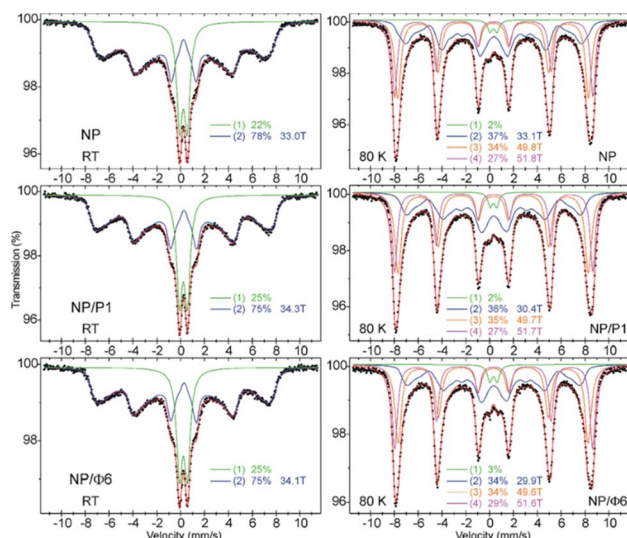**Fig. 5** ^{57}Fe Mössbauer spectra of NP, NP/P1, and NP/Φ6 samples measured at room temperature (left) and at 80 K (right). The relative area of respective spectral components is shown, and they correspond to: (1) – the superparamagnetic doublet, (2) – distribution of the magnetic sextets with the average magnetic field shown, and (3) and (4) – magnetic sextet with magnetic field shown.

Table 2 [57]Fe Mössbauer spectroscopy parameters of NP, NP/P1, and NP/Φ6 samples. The symbols: A – relative area of the respective spectral component corresponding to the relative contribution of Fe atoms into the respective iron state (phase), δ – isomer (center) shift relative to room temperature α-Fe, Δ – quadrupole splitting, B – hyperfine magnetic field, FWHM (full width at half maximum) – linewidth of the Lorentzian shaped spectral peak. Errors are of the order of unity for the last digit shown

Sample	T	A (%)	δ (mm s^{-1})	Δ (mm s^{-1})	B (Tesla)	FWHM (mm s^{-1})
NP	RT	22	0.33	0.64	—	0.58
		77	0.35	0	$\langle 33.0 \rangle$	$\langle 0.42 \rangle$
	80 K	2	0.43	0.58	—	0.48
		37	0.46	−0.01	$\langle 33.1 \rangle$	$\langle 0.58 \rangle$
		34	0.41	−0.02	49.8	0.62
		27	0.45	0	51.8	0.50
NP/P1	RT	25	0.34	0.66	—	0.58
		75	0.36	−0.01	$\langle 34.3 \rangle$	$\langle 0.42 \rangle$
	80 K	2	0.43	0.54	—	0.46
		36	0.45	−0.01	$\langle 30.4 \rangle$	0.68
		35	0.41	−0.02	49.7	0.66
		27	0.45	0.01	51.7	0.50
NP/Φ6	RT	25	0.33	0.66	—	0.60
		75	0.35	−0.02	$\langle 34.1 \rangle$	$\langle 0.42 \rangle$
	80 K	3	0.43	0.62	—	0.48
		34	0.44	0	$\langle 29.9 \rangle$	$\langle 0.62 \rangle$
		34	0.41	−0.02	49.6	0.64
		29	0.45	0	51.6	0.52

Fig. 6 Sorption isotherms of bacteria on magnetic phage-modified nanoparticles.

the phenomenon of superparamagnetism. The remaining broad spectral component shows magnetic splitting and corresponds to relatively larger superparamagnetic nanoparticles but with an estimated size not exceeding 10 nm.[57] The area-weighted mean hyperfine magnetic fields (also considering the contribution of a quadrupole doublet) are basically the same and amount to 25.7 T for NP, NP/P1, and NP/Φ6 samples. This suggests that there are no differences between the average size of MNPs in the studied samples. In order to freeze the superparamagnetic relaxation of nanoparticles, we performed the Mössbauer measurements with cooling of the samples with liquid nitrogen to 80 K. As shown in Fig. 5, the spectra are almost completely magnetically split. At least four spectral components were distinguished with the hyperfine magnetic field given in Table 2. These fields should rather be considered as average values corresponding to various sizes of nanoparticles, bearing in mind that a higher magnetic field corresponds to a larger nanoparticles. The differences between the values of respective magnetic fields for individual samples, although insignificant, lead to important conclusions, which are described in detail in the discussion section.

3.2. Sorption of bacteria

The adsorption isotherms (Fig. 6) were plotted to compare the adsorption of Gram-positive and Gram-negative bacteria (the cell walls of these bacteria differ significantly one another) to MNPs. The Langmuir isotherm approximated the number of adsorbed bacteria quite well ($r > 0.95$) depending on the number of bacteria remaining in the suspension after the process (Fig. 6). It can be seen that the bacteria were adsorbed
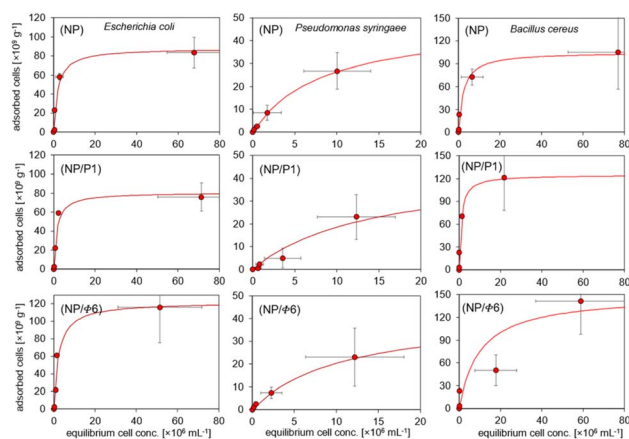
differently. Based on the Langmuir isotherm, the parameter A_{m} can be calculated to show how much bacteria can be maximally adsorbed on the MNPs (Table 3).

The highest sorption of *Escherichia coli* and *Bacillus cereus* occurred on the NP/Φ6, and amounted to 122 and 150×10^9 cells per g, respectively. The highest value for *P. syringae* occurred in NP (48.3×10^9 cells per g). However, the sorption of *Bacillus cereus* was higher in samples containing bacteriophages (NP/P1 and NP/Φ6), whereas the sorption of *P. syringae* on these samples was the weakest. The affinity of bacteria for the studied materials, expressed as the Langmuir constant (K_{L}), varied. However, the obtained values did not differ much clearly as for the A_{m} parameter (Table 3). The affinity of *E. coli* was highest for NP/P1 (0.67) in relation to NP and NP/Φ6 (0.5 and 0.43, respectively). The K_{L} parameter for *P. syringae* was the highest for NP (0.12), but the lowest value was observed for NP/P1 (0.07). In the case of *B. cereus*, the highest affinity was found at NP/P1 (1.03).

3.3. Electrokinetic potential of NP/QAS

MNPs with and without bacteriophages, as well as the QAS-modified MNPs, were analysed with the Zetameter to measure

Table 3 Parameters of sorption[a]

Bacteria	Sample	r	A_{m} [cells per g]	K_{L}
Escherichia coli	NP	0.97	87.8	0.5
	NP/P1	0.97	80.7	0.67
	NP/F6	0.97	122	0.43
Pseudomonas syringae	NP	0.99	48.3	0.12
	NP/P1	0.95	45	0.07
	NP/F6	0.99	42.8	0.09
Bacillus cereus	NP	0.99	105	0.43
	NP/P1	0.99	125	1.03
	NP/F6	0.98	150	0.1

[a] Abbreviations: r – correlation coefficient, A_{m} – maximum adsorption of bacteria, K_{L} – Langmuir constant interpreted as affinity of bacteria to adsorbent.
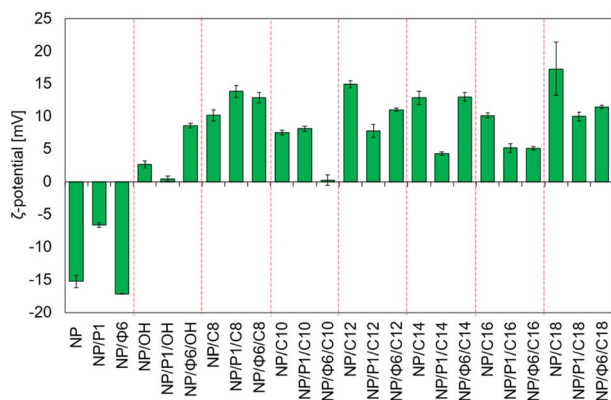
Fig. 7 ζ-Potential of MNPs.

ζ-potential (Fig. 7). The measured ζ-potential was negative for non-modified MNPs, and bacteriophage-based MNPs. The lowest value was noted for NP/Φ6 (ca. −17.0 mV). The ζ-potential for QAS-modified MNPs was always positive or close to 0 mV. The highest value was noted for NP/C18 and NP/C12, +17.3 mV and +14.9 mV, respectively. For QAS-bacteriophage-modified MNPs, the ζ-potential varied from +0.28 mV to +13.87 mV for NP/Φ6/C10 and NP/P1/C8, respectively.

The relationship between the values of the ζ-potential and the series of quaternary ammonium salts that modify the nanoparticles is not clearly visible. However, significant differences were found between the values of ζ-potential. The Dunnett's test (Table S2†) was used to compare several groups with a control sample. As a control group, samples NP, NP/P1, and

NP/Φ6 were chosen. The Scheffé test was used to assign samples to homogeneous groups in terms of ζ-potential (Table S2†).

3.4. Loss of viability of bacteria in presence of NP/QAS

The loss of viability of free-living *E. coli* did not change significantly in the presence of NP, NP/P1, NP/Φ6, and QAS-modified MNPs with OH – C14 ionic liquid precursors (Fig. 8a). NP/P1 caused an increase in the loss of viability of the adsorbed cells compared to the control sample (NP). NP/P1/C12 and NP/Φ6/C12 caused a similar effect. However, the changes were insignificant (max. 20% loss of viability). In turn, NP/Φ6/C14 increased the loss of viability of adsorbed cells (ca. 35%), while the free-living bacteria remained alive at the control level. The loss of viability for the NP/C14 and NP/P1/C14 samples did not change. Much more significant changes were noted for NP/P1/C16 and NP/Φ6/C16, that caused a considerable increase in loss of viability (>90%) of adsorbed bacteria, while for free-living bacteria it was 40%. Furthermore, NP/C16 (non-phage-modified NP/QAS) did not cause such an effect. C18-modified MNPs have also revealed the toxic effect. However, the differences were not such great.

Similar studies with *B. cereus* were unambiguous (Fig. 8b). In general, the loss of viability of adsorbed cells increased when the MNPs were modified with bacteriophages. This effect was clearly visible for non-QAS-modified NP/P1 and NP/Φ6, as well as QAS-modified NP/Φ6/C8, NP/Φ6/C14 and bacteriophage-modified NP with C18. On the other hand, for C16-modified MNPs the change of the loss of viability was insignificant. The Scheffé test was used to assign samples to homogeneous groups
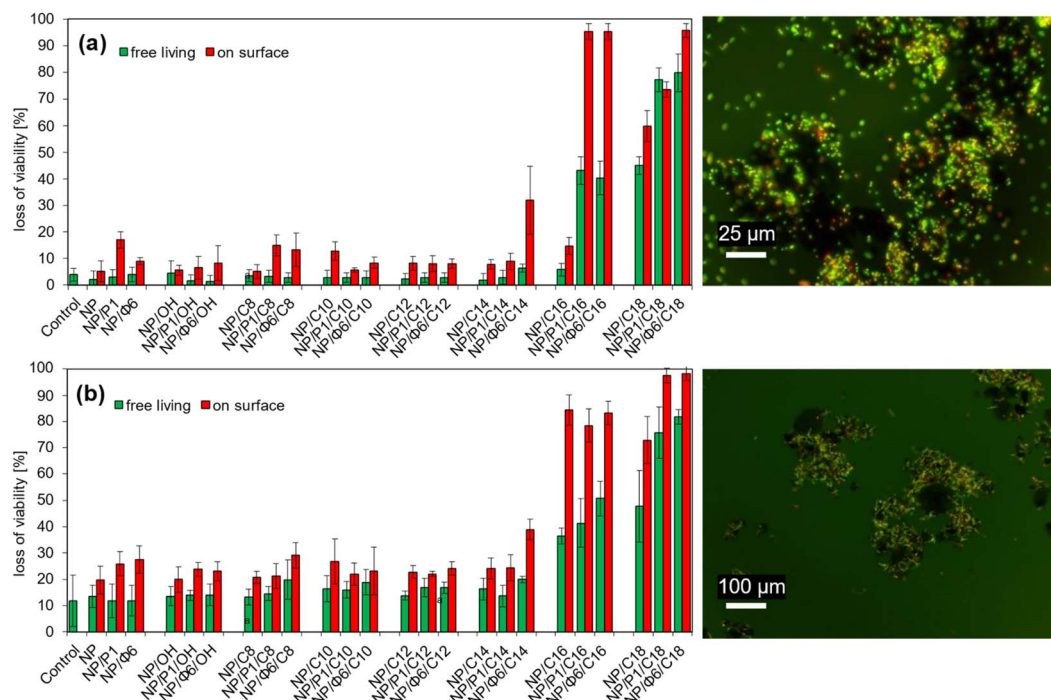

Fig. 8 Loss of viability after sorption of bacteria onto MNPs modified with ionic liquid precursors and/or bacteriophages. (a) – *Escherichia coli*; (b) – *Bacillus cereus*. Example of epifluorescence microscopic images after live/death staining (green/red) are also presented (right).

in terms of the loss of viability (Table S3 for *E. coli*, Table S4† for *B. cereus*).

3.5. Viability of bacteriophages attached to MNPs

The double-layer agar test did not show the characteristic plaques (bald spots), which are indicators of the viability of bacteriophages.

4. Discussion

XRD spectra and Mössbauer spectroscopy have revealed that maghemite was formed in all three samples (NP, NP/P1, NP/Φ6). No differences in maghemite/magnetite composition have been found among the samples. Our results are consistent with the spectra obtained by Sun *et al.*[53] The dominance of maghemite in the obtained samples may be related to the conditions of nanoparticle synthesis and the temperature used. Usually, the synthesis of magnetic nanoparticles by co-precipitation is carried out at temperatures close to 60 °C, which leads to the preparation of magnetite nanoparticles doped with maghemite. Then, the annealing of magnetite nanoparticles leads to a mixture of maghemite (γ-Fe$_2$O$_3$) and hematite (α-Fe$_2$O$_3$) affecting the magnetic properties.[54] However, in our research, annealing would destroy the structure of phage capsids, while the synthesis temperature close to 60 °C could be too high for the structure of bacterial viruses, especially for Φ6 phage whose capsids are covered with a lipid envelope. Therefore, the temperature was lowered to 40 °C. We used the measurement protocol known as the 'center of gravity' method, which has been developed to use ^{57}Fe Mössbauer spectrometry to measure the magnetite/maghemite ratio in iron-oxide-based MNPs.[55,56] The area-weighted mean isomer shifts of the spectra at RT are almost the same and amount to 0.35 mm s^{-1} for NP, NP/P1, and NP/Φ6. It indicates that the MNPs are mainly in the form of maghemite, with an estimated magnetite content of about 10%. It should be noted that the oxidation of magnetite nanoparticles to maghemite is assumed to be 'from the inside out'. This means that oxidation does not occur by oxygen diffusing into the particle but rather by the diffusion of iron ions out of the particle.[57] At 80 K, almost the entire spectrum is magnetically split, and more than 60% of the spectral area has a well-defined magnetic field up to 50 T or more, typical for bulk maghemite (as well as for magnetite). This means that about 60% of the Fe atoms are in relatively larger nanoparticles with blocked super-paramagnetism phenomenon, but the rest (40%) are still superparamagnetic. An interesting result is the calculation of the area of the weighted magnetic field mean. The values are as follows: 43.3 T for NP, 42.2 T for both NP/P1 and NP/Φ6 samples. This significant difference of over 1T (significantly exceeding the measurement uncertainty) clearly indicates some physical change in the structure of MNPs under the influence of bacteriophages. One of the most likely explanations is the influence of bacteriophages to hinder the clustering (growth) of nanoparticles, which leads to a reduced hyperfine magnetic field. It should be noted that Mössbauer spectroscopy measurements at low temperatures increase the sensitivity of the method to the size of MNPs. The area-weighted mean isomer shift of the spectra at 80 K amount to 0.44 mm s^{-1} for NP, NP/P1, and NP/Φ6 confirm that the nanoparticles are mainly in the form of maghemite.[55]

Bacteriophages are supposed to be covered by nanoparticles. Bacteriophages were not visible in SEM images, possibly due to the tight coating of their surface with MNPs, while bacteriophages were highly visible in epifluorescence microscopy after staining. Importantly, it seems that the bacteriophages altered the properties of the MNPs. The sorption experiments showed the maximum sorption of bacteria (level of sorption). However, the maximum number of adsorbed bacteria does not indicate the affinity of bacterial cells to the surface of MNPs. Thus, the Langmuir constant can be used to measure the affinity. Hence, these parameters should be considered together for better characterization of the bacterial sorption. It is clearly visible that bacteriophages affected the sorption of bacteria, especially for *B. cereus*. The presence of bacteriophages caused a significant increase in the number of adsorbed cells for *E. coli* and *B. cereus*, but it was not always followed by their affinity for the bacteriophage-based nanoparticles. On the other hand, such an effect was not noted in *P. syringae*. Surprisingly, the effect of the increased affinity of bacteriophage-based MNPs for the host bacteriophage is difficult to assess. This phenomenon may have occurred with *E. coli* and NP/P1, where an increase in the affinity of the cells for MNPs was observed. On the other hand, this effect was not found with *P. syringae*. Supposedly, the presence of Φ6 bacteriophage could have significantly modified the sorption of bacteria through the presence of a lipid envelope.

MacRae and Evans described the sorption of bacteria on magnetite nanoparticles.[58] They used *Escherichia coli* UQM70 with a concentration of 7.17×10^6 cfu mL^{-1}; 200 mL of a solution and 1% of nanoparticles. Their efficiency was about 99%. Our results are in agreement with their findings. The sorption of bacteria on MNPs has been highly efficient. In general, the values of A_m for *E. coli* and *B. cereus* are much higher than those for *P. syringae*. Nonetheless, it seems that the size of the bacteria does not play a crucial role. The diameter is 1–2,[59] 1.5,[60] 3–5 μm,[61] for *E. coli*, *P. syringae*, and *B. cereus* respectively. It is assumed that *E. coli* and *B. cereus* might have a better affinity to the lipid envelope of the Φ6 bacteriophages. Unlike previous bacteria, *P. syringae* has a worse affinity, and the fact might be caused due to the fact, that the envelope of the Φ6 bacteriophage is built from the cell membrane components of their host,[62] and therefore repulse.

The change in the properties of bacteriophage-modified MNPs was perfectly revealed in the experiments with QAS-modified MNPs. It was checked whether the QAS- and bacteriophage-modified MNPs can affect the viability of bacteria attached to the surface. It was shown above that the electrokinetic potential changed when QAS modified the MNPs. Hence, it can be assumed that the positive net surface charge of NP/QAS should affect the sorption of bacteria. Following, the loss of viability of adsorbed cells can increase when the length of alkyl chain of QAS elongates.

This is very clearly visible in the results of the loss-of-viability test. First, bacteriophages can increase the loss of *E. coli* viability. Second, the presence of Φ6 bacteriophage lipid envelope in Φ6/NP modified by QAS C14, C16, and C18 significantly increased the loss of viability of cells adsorbed on the surface of such materials. Therefore, it was possible that the lipid envelope of Φ6 bacteriophage interacted with QAS. This effect is confirmed by the control samples (NP/C14 and NP/C16), where the antibacterial effect was barely noted.

Moreover, more toxic QASs (with longer chains), which modify MNPs in the presence of bacteriophages, seem to have better antibacterial properties in comparison to the QAS-modified MNPs without bacteriophages. This effect is less visible with *B. cereus*, but Gram-positive bacteria are generally much more sensitive to the presence of ionic liquids and their precursors,[48,49,63–66] thus the effect of bacteriophages can be masked. On the other hand, Gram-negative bacteria are more resistant to QAS, so the effect of increased toxicity of QAS-modified bacteriophage-based MNPs can be easily visible. Moreover, the presence of QAS modifies the electrokinetic potential of MNPs with and without bacteriophages.

The proposed mechanism of action of the QAS-bacteriophage-modified MNPs is presented in Fig. 9. QAS are probably linked to the surface of bacteriophages. Subsequently, precipitation of MNPs occurs. Then, agglomerates of MNPs and bacteriophages are formed. Due to the presence of QAS, some modifications of the antibacterial properties are revealed. Especially for lipid-enveloped Φ6 bacteriophage. Importantly, agglomeration of mineral phases after precipitation with bacteriophages has already been suggested.[36,37] It is possible that similar mechanisms occur during the precipitation of MNPs in the presence of bacteriophages. Here, the potential for the construction of bacteriophage-modified MNPs opens up. MNPs may have desired properties, depending on the technological goals. Such particles can be used as better sorbents for microorganisms and materials with bactericidal properties.

Bacteriophages have been used as modifying agents so far. He *et al.* prepared magnetic beads conjugated to bacteriophages.[67] However, they used comparatively large (1.5 μm diameter) commercially available magnetic beds covered with toluenesulfonyl groups, while we synthesized smaller nanoparticles of one order of magnitude. From the point of view of drug carriers, smaller nanoparticles (<150 nm dimeter) are better because they can cross the endothelial barrier.[68] Furthermore, a synthesis can be cheaper than commercially available products. However, the viability test of viruses attached to the nanoparticles has shown that the viruses are not viable. The bacteriophages are supposed to be damaged during synthesis by alkali pH. Another hypothesis is that the bacteriophages are completely covered with nanoparticles, and viruses cannot attach to bacteria. We suppose that a different synthesis method (without harsh reagents) may provide better results. However, combining our synthesis with the phage-display method (expression of desired peptides on the surface of bacteriophages[69]) could provide a basis for further research, especially in terms of drug delivery systems, where the viability of bacteriophages is not necessary. You *et al.* proposed a method to attach bacteriophages to the surface of MNPs.[70] Their method is entirely different from our approach. They used various chemical compounds that modified the surface of commercially available nanoparticles and subsequently added bacteriophages to the mixture. On the other hand, we combined the synthesis of MNPs and the linking of bacteriophages in one step.

Magnetic nanoparticles coated with viruses and functionalized with precursors of ionic liquids have different antibacterial properties. Our results are consistent with those obtained by Borkowski *et al.*[49] Nanoparticles functionalized with ILs, which have long acryl chains, have better antibacterial properties. It should be noted that some nanoparticles covered with viruses changed their antibacterial activity. Markiewicz *et al.*[71] studied the adsorption of ILs on quartz and kaolinite. They described the reversal of mineral charge by the adsorption of several ionic liquids. Their ζ-potential measurement results are consistent with our findings. Here, ILs precursors tend to change the surface of MNPs, and thus the electrokinetic potential. It should be noted that the presence of viruses can drastically change the charge of the surface. Statistical analysis has shown that most samples differ significantly from the control sample. We can assume that the bacteriophages change the affinity of ILs precursors for MNPs.
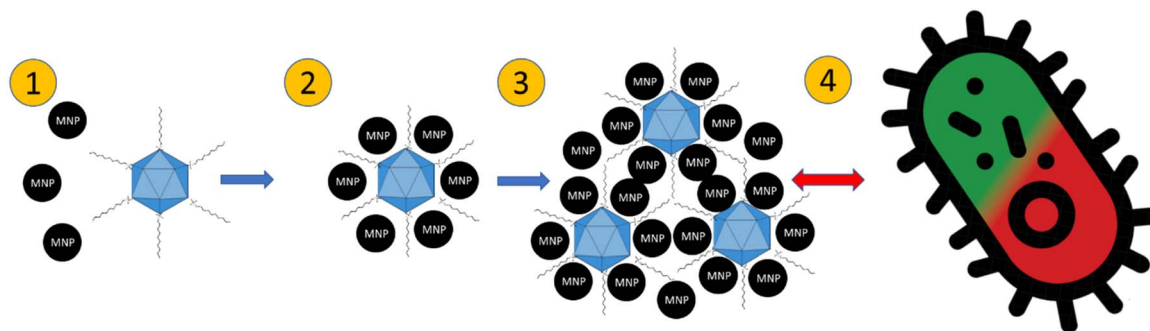

Fig. 9 A hypothetical process of the formation of QAS-bacteriophage-MNPs complexes and their antibacterial mechanism of action. (1) Attachment of MNPs to QAS-modified bacteriophages; (2) bacteriophages are covered with MNPs; (3) agglomeration of bacteriophage-MNPs complexes; (4) interaction with bacteria resulting in a change in the loss of viability.

5. Conclusions

In this work, we have presented the synthesis of composites based on bacteriophages (*Escherichia* phage P1 and *Pseudomonas* phage Φ6), magnetic nanoparticles, and ionic liquids precursors. The sorption and antibacterial effect of QAS-modified MNPs have also been investigated. SEM imaging has not revealed any significant differences in the morphology of the minerals obtained. Epifluorescence microscopy has also not revealed any significant differences in the agglomeration of nanoparticles but has shown a strong attachment of MNPs to bacteriophages. The results of XRD and Mössbauer spectroscopy have confirmed the presence of iron oxide nanoparticles in maghemite/magnetite form among the samples. Bacteriophages caused some physical changes in the structure of MNPs, which had the effect of reducing the hyperfine magnetic field. It is assumed that bacteriophages may hinder the growth of nanoparticles. The presence of bacteriophages changed the surface potential of the prepared samples. Sorption studies towards *E. coli*, *P. syringae* and *B. cereus* have also shown that the bacteriophages change the properties of MNPs. It can be concluded that the viability of the adsorbed bacteria depends on the length of the *n*-alkyl chain when the samples are modified with QAS. Generally, it was observed that the increase in the loss of viability was higher for *E. coli* than for *P. syringae*. Our studies present the potential of the QAS- and bacteriophage-modified MNPs as promising antibacterial agents.

Author contributions

PD and AB designed and conducted the experiments, analysed the data, and wrote the manuscript; ABł performed Mössbauer spectroscopy measurements, MDS performed SEM analyses; TB performed XRD analyses, KK performed the ζ-potential measurements; MO and ŁZ contributed to writing the article.

Conflicts of interest

There are no conflicts to declare.

Acknowledgements

References

1 A. G. Roca, L. Gutiérrez, H. Gavilán, M. E. Fortes Brollo, S. Veintemillas-Verdaguer and M. d. P. Morales, *Adv. Drug Delivery Rev.*, 2019, **138**, 68–104.

2 R. A. Revia and M. Zhang, *Mater. Today*, 2016, **19**, 157–168.

3 A. Hernando, P. Crespo and M. A. García, *Sci. World J.*, 2005, **5**, 972–1001.

4 S. V. German, N. A. Navolokin, N. R. Kuznetsova, V. V. Zuev, O. A. Inozemtseva, A. A. Anis'kov, E. K. Volkova, A. B. Bucharskaya, G. N. Maslyakova, R. F. Fakhrullin, G. S. Terentyuk, E. L. Vodovozova and D. A. Gorin, *Colloids Surf., B*, 2015, **135**, 109–115.

5 C. Y. Haw, F. Mohamed, C. H. Chia, S. Radiman, S. Zakaria, N. M. Huang and H. N. Lim, *Ceram. Int.*, 2010, **36**, 1417–1422.

6 M. Khalkhali, S. Sadighian, K. Rostamizadeh, F. Khoeini, M. Naghibi, N. Bayat, M. Habibizadeh and M. Hamidi, *BioImpacts*, 2017, **5**, 141–150.

7 M. Fazilati, *Cell Biol. Int.*, 2014, **38**, 154–163.

8 A. Rao, A. Bankar, A. R. Kumar, S. Gosavi and S. Zinjarde, *J. Contam. Hydrol.*, 2013, **146**, 63–73.

9 A. Abbasi Kajani and A.-K. Bordbar, *J. Hazard. Mater.*, 2019, **366**, 268–274.

10 W. Jiang, M. Pelaez, D. D. Dionysiou, M. H. Entezari, D. Tsoutsou and K. O'Shea, *Chem. Eng. J.*, 2013, **222**, 527–533.

11 A. Idris, N. S. M. Ismail, N. Hassan, E. Misran and A.-F. Ngomsik, *J. Ind. Eng. Chem.*, 2012, **18**, 1582–1589.

12 E. M. Múzquiz-Ramos, V. Guerrero-Chávez, B. I. Macías-Martínez, C. M. López-Badillo and L. A. García-Cerda, *Ceram. Int.*, 2015, **41**, 397–402.

13 R. Kumar, R. Sakthivel, R. Behura, B. K. Mishra and D. Das, *J. Alloys Compd.*, 2015, **645**, 398–404.

14 F. Fajaroh, H. Setyawan, W. Widiyastuti and S. Winardi, *Adv. Powder Technol.*, 2012, **23**, 328–333.

15 V. M. Lenart, R. de Fátima Turchiello, M. P. Calatayud, G. F. Goya and S. L. Gómez, *Braz. J. Phys.*, 2019, **49**, 829–835.

16 A. Watcharenwong, Y. Bailuang and P. Kajitvichyanukul, *Key Eng. Mater.*, 2017, **737**, 367–372.

17 V. Akinwekomi, J. P. Maree, C. Zvinowanda and V. Masindi, *J. Environ. Chem. Eng.*, 2017, **5**, 2699–2707.

18 S. Sun and H. Zeng, *J. Am. Chem. Soc.*, 2002, **124**, 8204–8205.

19 E. Darezereshki, *Mater. Lett.*, 2010, **64**, 1471–1472.

20 W. Gawęda, M. Osial, M. Żuk, M. Pękała, A. Bilewicz and P. Krysinski, *Nanomaterials*, 2020, **10**, 288.

21 A. Bee, R. Massart and S. Neveu, *J. Magn. Magn. Mater.*, 1995, **149**, 6–9.

22 S. Yoon, *J. Magn. Soc. Jpn.*, 2014, **19**, 323–326.

23 J. Y. Park, E. S. Choi, M. J. Baek and G. H. Lee, *Mater. Lett.*, 2009, **63**, 379–381.

24 X. N. Pham, T. P. Nguyen, T. N. Pham, T. T. N. Tran and T. V. T. Tran, *Adv. Nat. Sci.: Nanosci. Nanotechnol.*, 2016, **7**, 045010.

25 M. Ebadi, K. Buskaran, S. Bullo, M. Z. Hussein, S. Fakurazi and G. Pastorin, *Polymers*, 2020, **12**, 2716.

26 R. A. Bini, R. F. C. Marques, F. J. Santos, J. A. Chaker and M. Jafelicci, *J. Magn. Magn. Mater.*, 2012, **324**, 534–539.

27 M. Abbas, B. Parvatheeswara Rao, S. M. Naga, M. Takahashi and C. Kim, *Ceram. Int.*, 2013, **39**, 7605–7611.

28 D. Chełminiak, M. Ziegler-Borowska and H. Kaczmarek, *Mater. Lett.*, 2016, **164**, 464–467.

29 K. D. Wani, B. S. Kadu, P. Mansara, P. Gupta, A. V. Deore, R. C. Chikate, P. Poddar, S. D. Dhole and R. Kaul-Ghanekar, *PLoS One*, 2014, **9**, e107315.

30 E. Maltas, M. Ozmen, H. C. Vural, S. Yildiz and M. Ersoz, *Mater. Lett.*, 2011, **65**, 3499–3501.

31 A. K. Bordbar, A. A. Rastegari, R. Amiri, E. Ranjbakhsh, M. Abbasi and A. R. Khosropour, *Biotechnol. Res. Int.*, 2014, **2014**, 1–6.

32 M. Babič, D. Horák, P. Jendelová, K. Glogarová, V. Herynek, M. Trchová, K. Likavčanová, P. Lesný, E. Pollert, M. Hájek and E. Syková, *Bioconjugate Chem.*, 2009, **20**, 283–294.

33 T.-H. Hsieh, K.-S. Ho, X. Bi, Y.-K. Han, Z.-L. Chen, C.-H. Hsu and Y.-C. Chang, *Eur. Polym. J.*, 2009, **45**, 613–620.

34 E. Corem-Salkmon, Z. Ram, D. Daniels, B. Perlstein, D. Last, S. Salomon, G. Tamar, R. Shneor, D. Guez, S. Margel and Y. Mardor, *Int. J. Nanomed.*, 2011, **6**, 1595–1602.

35 C. P. Devatha and S. Shivani, *J. Environ. Manage.*, 2020, **258**, 110038.

36 M. Słowakiewicz, A. Borkowski, M. D. Syczewski, I. D. Perrota, F. Owczarek, A. Sikora, A. Detman, E. Perri and M. E. Tucker, *Geochim. Cosmochim. Acta*, 2021, **292**, 482–498.

37 P. Działak, M. D. Syczewski, K. Kornaus, M. Słowakiewicz, Ł. Zych and A. Borkowski, *Biogeosciences*, 2022, **19**, 4533–4550.

38 R. D. Rogers and K. R. Seddon, *Science*, 2003, **302**, 792–793.

39 S. A. Forsyth, J. M. Pringle and D. R. MacFarlane, *Aust. J. Chem.*, 2004, **57**, 113.

40 K. Ghandi, *Green Sustainable Chem.*, 2014, **04**, 44–53.

41 D. D. Patel and J.-M. Lee, *Chem. Rec.*, 2012, **12**, 329–355.

42 T. Welton, *Coord. Chem. Rev.*, 2004, **248**, 2459–2477.

43 J. Lu, F. Yan and J. Texter, *Prog. Polym. Sci.*, 2009, **34**, 431–448.

44 C. Roosen, P. Müller and L. Greiner, *Appl. Microbiol. Biotechnol.*, 2008, **81**, 607–614.

45 A. Borkowski, Ł. Gutowski, M. Syczewski, T. Cłapa and G. Czerwonka, *Ecotoxicol. Environ. Saf.*, 2018, **164**, 370–378.

46 N. V. Plechkova and K. R. Seddon, *Chem. Soc. Rev.*, 2008, **37**, 123–150.

47 A. Borkowski, Ł. Ławniczak, T. Cłapa, D. Narożna, M. Selwet, D. Pęziak, B. Markiewicz and Ł. Chrzanowski, *Ecotoxicol. Environ. Saf.*, 2016, **130**, 54–64.

48 P. Kowalczyk, A. Borkowski, G. Czerwonka, T. Cłapa, J. Cieśla, A. Misiewicz, M. Borowiec and M. Szala, *J. Mol. Liq.*, 2018, **266**, 540–547.

49 A. Borkowski, P. Kowalczyk, G. Czerwonka, J. Cieśla, T. Cłapa, A. Misiewicz, M. Szala and M. Drabik, *J. Mol. Liq.*, 2017, **246**, 282–289.

50 L. A. Day and R. L. Wiseman, *Cold Spring Harb.*, 1978, **08**, 605–625.

51 M. B. Łobocka, D. J. Rose, G. Plunkett, M. Rusin, A. Samojedny, H. Lehnherr, M. B. Yarmolinsky and F. R. Blattner, *J. Bacteriol.*, 2004, **186**, 7032–7068.

52 B. E. Ford, PhD thesis, City University of New York, 2015.

53 Y. Sun, M. Ma, Y. Zhang and N. Gu, *Colloids Surf., A*, 2004, **245**, 15–19.

54 M. Ounacer, A. Essoumhi, M. Sajieddine, A. Razouk, B. F. O. Costa, S. M. Dubiel and M. Sahlaoui, *J. Supercond. Novel Magn.*, 2020, **33**, 3249–3261.

55 J. Fock, L. K. Bogart, D. González-Alonso, J. I. Espeso, M. F. Hansen, M. Varón, C. Frandsen and Q. A. Pankhurst, *J. Phys. D: Appl. Phys.*, 2017, **50**, 265005.

56 L. K. Bogart, J. Fock, G. M. da Costa, K. Witte, J.-M. Greneche, J. Zukrowski, M. Sikora, D. E. Latta, M. M. Scherer, M. F. Hansen, C. Frandsen and Q. A. Pankhurst, *Metrologia*, 2022, **59**, 015001.

57 L. K. Bogart, C. Blanco-Andujar and Q. A. Pankhurst, *Appl. Phys. Lett.*, 2018, **113**, 133701.

58 I. C. MacRae and S. K. Evans, *Water Res.*, 1984, **18**, 1377–1380.

59 Z. W. El-Hajj and E. B. Newman, *Front. Microbiol.*, 2015, **6**, 1–12.

60 B. S. Thind, *Phytopathogenic Bacteria and Plant Diseases*, CRC Press, Taylor & Francis, Boca Raton, 1st edn, 2019.

61 L. P. Stenfors Arnesen, A. Fagerlund and P. E. Granum, *FEMS Microbiol. Rev.*, 2008, **32**, 579–606.

62 O. L. Lyytinen, D. Starkova and M. M. Poranen, *Microb. Cell Fact.*, 2019, **18**, 29.

63 A. N. Duman, I. Ozturk, A. Tunçel, K. Ocakoglu, S. G. Colak, M. Hoşgör-Limoncu and F. Yurt, *Heliyon*, 2019, **5**, e02607.

64 M. Sivapragasam, M. Moniruzzaman and M. Goto, *Biotechnol. J.*, 2020, **15**, 1900073.

65 R. Popescu, M. N. Filimon, D. C. Vlad, D. Verdes, A. Moatar, G. Moise, K. Guran, I. V. Caraba, L. P. Ciochina, I. Pinzaru, C. A. Dehelean and G. Dumitrescu, *Exp. Ther. Med.*, 2021, **22**, 1–9.

66 K. M. Docherty and J. C. F. Kulpa, *Green Chem.*, 2005, **7**, 185–189.

67 Y. He, M. Wang, E. Fan, H. Ouyang, H. Yue, X. Su, G. Liao, L. Wang, S. Lu and Z. Fu, *Anal. Chem.*, 2017, **89**, 1916–1921.

68 M. Gaumet, A. Vargas, R. Gurny and F. Delie, *Eur. J. Pharm. Biopharm.*, 2008, **69**, 1–9.

69 J. Pande, M. M. Szewczyk and A. K. Grover, *Biotechnol. Adv.*, 2010, **28**, 849–858.

70 F. You, G. Yin, X. Pu, Y. Li, Y. Hu, Z. Huang, X. Liao, Y. Yao and X. Chen, *Colloids Surf., B*, 2016, **141**, 537–545.

71 M. Markiewicz, W. Mrozik, K. Rezwan, J. Thöming, J. Hupka and C. Jungnickel, *Chemosphere*, 2013, **90**, 706–712.